doi:10.1016/j.jmb.2010.06.049 J. Mol. Biol. (2010) 401, 544–551

JMB

Available online at www.sciencedirect.com

ScienceDirect

ELSEVIER

Helical Filaments of Human Dmc1 Protein on Single-Stranded DNA: A Cautionary Tale

Xiong Yu and Edward H. Egelman*

Department of Biochemistry and Molecular Genetics, Box 800733, University of Virginia, Charlottesville, VA 22908-0733, USA

Received 28 May 2010; received in revised form 16 June 2010; accepted 23 June 2010
Available online 30 June 2010

Proteins in the RecA/Rad51/RadA family form nucleoprotein filaments on DNA that catalyze a strand exchange reaction as part of homologous genetic recombination. Because of the centrality of this system to many aspects of DNA repair, the generation of genetic diversity, and cancer when this system fails or is not properly regulated, these filaments have been the object of many biochemical and biophysical studies. A recent paper has argued that the human Dmc1 protein, a meiotic homolog of bacterial RecA and human Rad51, forms filaments on single-stranded DNA with ~9 subunits per turn in contrast to the filaments formed on double-stranded DNA with ~6.4 subunits per turn and that the stoichiometry of DNA binding is different between these two filaments. We show using scanning transmission electron microscopy that the Dmc1 filament formed on single-stranded DNA has a mass per unit length expected from ~6.5 subunits per turn. More generally, we show how ambiguities in helical symmetry determination can generate incorrect solutions and why one sometimes must use other techniques, such as biochemistry, metal shadowing, or scanning transmission electron microscopy, to resolve these ambiguities. While three-dimensional reconstruction of helical filaments from EM images is a powerful tool, the intrinsic ambiguities that may be present with limited resolution are not sufficiently appreciated.

© 2010 Elsevier Ltd. All rights reserved.

Keywords: electron microscopy; helical polymers; three-dimensional reconstruction

Edited by W. Baumeister

Introduction

Homologous genetic recombination involves the exchange of DNA strands between two DNA molecules that share extensive sequence identity. The bacterial RecA protein has long served as a model[1] for how protein-mediated homologous recombination can take place *in vivo* and *in vitro*. We now understand that all three kingdoms of life encode RecA-like proteins, with RecA in prokaryotes, RadA in archaea,[2] and Rad51 in eukaryotes.[3] The eukaryotic Dmc1 protein has been shown[4] to be another RecA homolog, involved in meiotic recombination. Because of the centrality of these proteins to such processes as DNA repair, an extensive literature exists on the biochemical and structural characterization of the helical filaments formed by these proteins on DNA that mediate the recognition of homology between two similar DNA molecules and catalyze a strand exchange between these two molecules.

A recent paper[5] has argued, using image analysis of electron microscopic images, that filaments formed by the human Dmc1 (hDmc1) protein on single-stranded DNA (ssDNA) have ~9 subunits per turn of the helix, while filaments formed on double-stranded DNA (dsDNA) have ~6.4 subunits per turn. We have previously shown[6] that the filaments of hDmc1 on dsDNA have ~6.4 subunits per turn; hence, the low-resolution structure of those hDmc1-dsDNA filaments appears similar to filaments formed by homologous proteins such as bacterial RecA,[7] eukaryotic Rad51,[8] and archaeal RadA.[8] However, the following suggestion has been made:[5] that subunits in the hDmc1-ssDNA filament have a very different orientation from subunits in other RecA-like filaments studied thus

*Corresponding author. E-mail address: egelman@virginia.edu.

Abbreviations used: ssDNA, single-stranded DNA; dsDNA, double-stranded DNA; IHRSR, iterative helical real-space reconstruction; STEM, scanning transmission electron microscopy.

0022-2836/$ - see front matter © 2010 Elsevier Ltd. All rights reserved.

far and have a different stoichiometry of DNA binding: two bases per protein subunit in the hDmc1-ssDNA filament *versus* three bases or base pairs per subunit in all of the other filaments that have been extensively characterized. The most detailed picture that exists for the protein–DNA interface in these filaments comes from crystal structures[9] of the *Escherichia coli* RecA protein on both ssDNA and dsDNA, where the unusual extension and untwisting of DNA by these proteins is explained by triplets maintained in a normal right-handed B-like conformation followed by a left-handed twist and complete unstacking between triplets. The proposed stoichiometry of two bases per Dmc1 is in conflict with experimental observations showing that hDmc1 provides the same stoichiometric protection to ssDNA against nuclease digestion as the *E. coli* RecA protein.[10] The proposed structure of these hDmc1-ssDNA filaments can be directly tested, since the previous paper[5] makes a prediction that the mass per unit length of these filaments (having 9 subunits per turn, with each turn containing 18 bases) would be substantially greater than a "canonical" hDmc1-ssDNA filament (containing 6.4 subunits and 19.2 bases per turn).

Results

Electron microscopy of negatively stained specimens was used to look at hDmc1 filaments formed on dsDNA (Fig. 1a) and on ssDNA (Fig. 1b and c). In the presence of the non-hydrolyzable ATP analog AMP-PNP (Fig. 1a and b), the filaments display a very strong helical pattern caused by the deep groove. It has previously been shown that this ATP analog binds to hDmc1 filaments and maintains them in an extended state.[6] Using ATP and Ca^{2+} instead of AMP-PNP, under very similar conditions used by Okorokov *et al.*,[5] the filaments appear (Fig. 1c) to be much more flexible and "fuzzy". The filaments formed on long dsDNA molecules (Fig. 1a) can be thousands of Ångstroms in length. In contrast, a 108-mer single-stranded oligonucleotide has been used for Fig. 1b and c, and these oligonucleotides must stack together to form longer filaments, as only a few of the observed filaments correspond to the length of ~540 Å (or ~5–6 turns of the helix) expected for a filament formed on a 108-mer. Under the three different conditions used, ring-like structures are always present (Fig. 1a, arrow). We suggest that these are the same octameric rings previously described.[11]

Variable pitch

Analysis of the helical pitch of these three different forms (hDmc1-dsDNA-AMP-PNP, hDmc1-ssDNA-AMP-PNP, and hDmc1-ssDNA-ATP-Ca^{2+}) shows considerable variability (Fig. 2). Global three-dimensional reconstructions were made from each of these sets using the iterative helical real-space reconstruction (IHRSR) approach[13] forcing the subunit axial rise to be very small (1.0 Å) so that only the average density along the continuous one-start helix is preserved. These reconstructions were then deformed to have pitch values from 75 to 115 Å in 5-Å increments, creating nine reference volumes for each set. Examples are shown (Fig. 2f–h) for volumes having pitches of 80, 90, and 100 Å, respectively. A reference-based approach (using cross-correlations between projections of the nine reference volumes and the images of the filament segments) was then used to classify segments (each 74 pixels or ~310 Å long) by pitch, generating the histograms in Fig. 2a–c.

How reliable is this classification? Two different approaches were used to test this. We can assume that the variance of these distributions will have two underlying causes: intrinsic variance in the pitch, and error in assignment. For no variation in pitch, we might therefore expect a distribution with finite width just due to the presence of noise and errors in classification. However, power spectra from different bins would then show a layer line at the same position, and this is not the case. Figure 2d and e show the averaged power spectra from segments classified in Fig. 2c (hDmc1-ssDNA-ATP-Ca^{2+}) as having either 85 or 105 Å pitch, respectively. Since such averaged power spectra are invariant under any translations of the image segments, they are not susceptible to the artifacts associated with the averaging of images. Power spectra were generated from every bin (data not shown), and each displayed a layer line at the position expected from the classification.

A second approach involves the use of a "reference-free" algorithm for generating averaged images.[12] When this method is applied to the segments classified in Fig. 2c as having 80, 90, or 100 Å pitch, the resulting averages (Fig. 2i–k, respectively) show the difference in pitch expected.

The pitch histograms (Fig. 2) show that all filaments appear to have a continuous distribution of pitch and that the filaments formed on ssDNA with ATP and Ca^{2+} have the broadest distribution. In contrast, Okorokov *et al.* stated that they could classify their segments (formed under similar conditions with ATP and Ca^{2+}) as having a pitch of either ~110 Å (the "extended" state) or ~96 Å (the "compressed" state).

STEM analysis

We have used scanning transmission electron microscopy (STEM) to directly measure[14] the mass per unit length of hDmc1-ssDNA filaments (Fig. 3). Filaments prepared with AMP-PNP (Fig. 3a) are preserved fairly well after the adsorption to a carbon film, washing, and freeze-drying used in STEM preparations. An averaged power spectrum generated from 13 segments of such unstained freeze-dried hDmc1-ssDNA-AMP-PNP filaments (Fig. 3b) shows a pitch of ~100 Å. The layer line is strongly one-sided, suggesting that the side of the filament

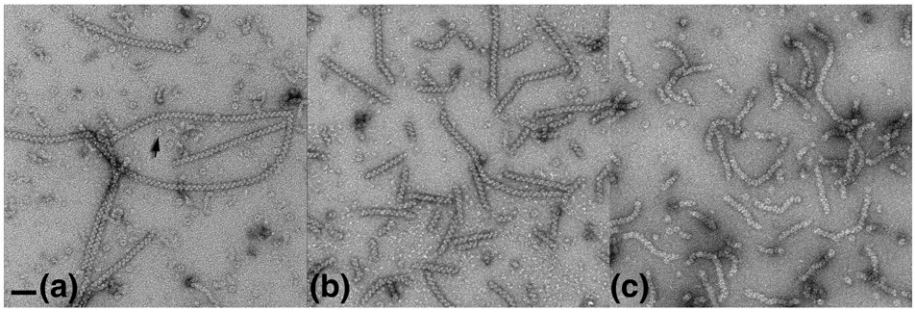


Fig. 1. Electron microscopic images of negatively stained hDmc1-dsDNA filaments (a) and hDmc1-ssDNA filaments (b and c). The filaments in (a) and (b) were prepared with the non-hydrolyzable ATP analog, AMP-PNP. The filaments in (c) were prepared with ATP and Ca^{2+}. Under all conditions, ring-like structures can be seen (arrow, a). The scale bar in (a) represents 500 Å.

adsorbed to the carbon support film has largely collapsed. However, such a collapse would not affect mass measurements. The average mass/length measured (Fig. 3c), 2.6±0.2 (SD) kDa/Å, is extremely close to that predicted for 6.4 subunits turn containing 19.2 bases (2.5 kDa/Å) and inconsistent with a model for 9 subunits with 18 bases (3.5 kDa/Å). The asymmetry in the shape of the mass distribution (Fig. 3c) may result from the fact that care was taken to only include segments where a strong helical striation was visible. Collapsed segments, showing no helical pitch, have a higher mass per unit length (data not shown). While the mass distribution is broad, there is no overlap with the predicted[5] higher mass/length.

In contrast to the AMP-PNP filaments, those formed with ATP and Ca^{2+} fall apart during preparation for STEM imaging (Fig. 3d). This is consistent with earlier observations[15] where it was noted that such filaments also fell apart when prepared for

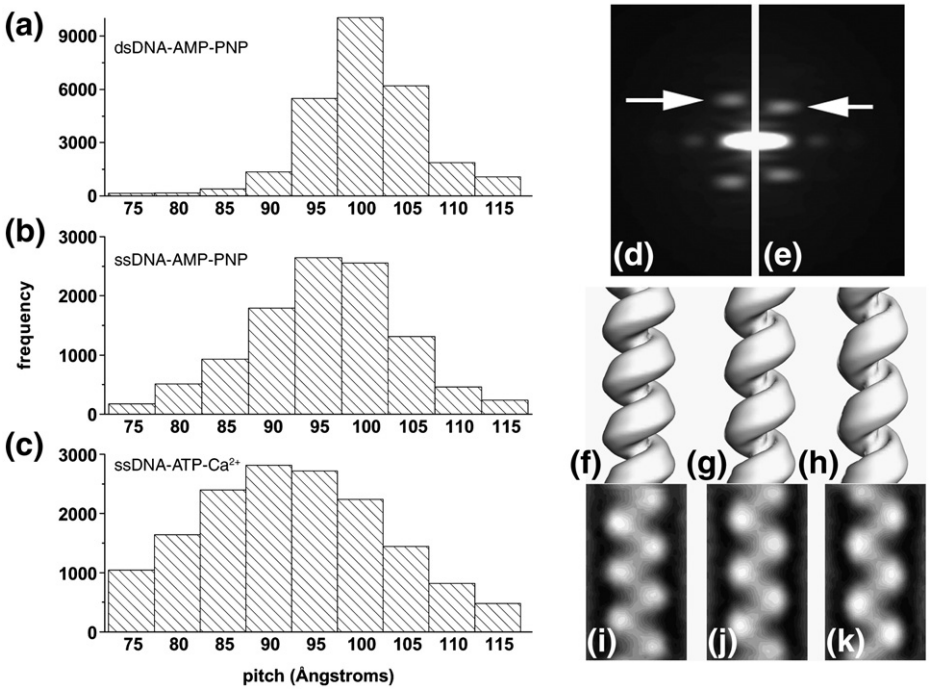


Fig. 2. Cross-correlations against projections of different reference volumes were used to sort segments by pitch (a–c). The distribution in (a) is for the hDmc1-dsDNA-AMP-PNP filaments, that in (b) is for the hDmc1-ssDNA-AMP-PNP filaments, and that in (c) is for the hDmc1-ssDNA-ATP-Ca^{2+} filaments. The validity of the sorting was confirmed by showing that the averaged power spectra from segments in each bin showed a layer line that shifted as expected. For example, the averaged power spectrum (d) from segments in the 85-Å bin (c) has a layer line at ~1/(85 Å), while the averaged power spectrum (e) from segments in the 105-Å bin has a layer line at ~1/(105 Å). Examples are shown (f–h) for the three-dimensional volumes used to do the cross-correlation sorting. These volumes have a pitch of 80 Å (f), 90 Å (g), and 100 Å (h). The "reference-free" averages[12] of hDmc1-ssDNA-ATP-Ca^{2+} segments (c) from the bins labeled 80, 90, and 100 Å are shown in (i)–(k), respectively. It can be seen that these averages show the continuous variation in pitch as suggested by the distribution in (c).

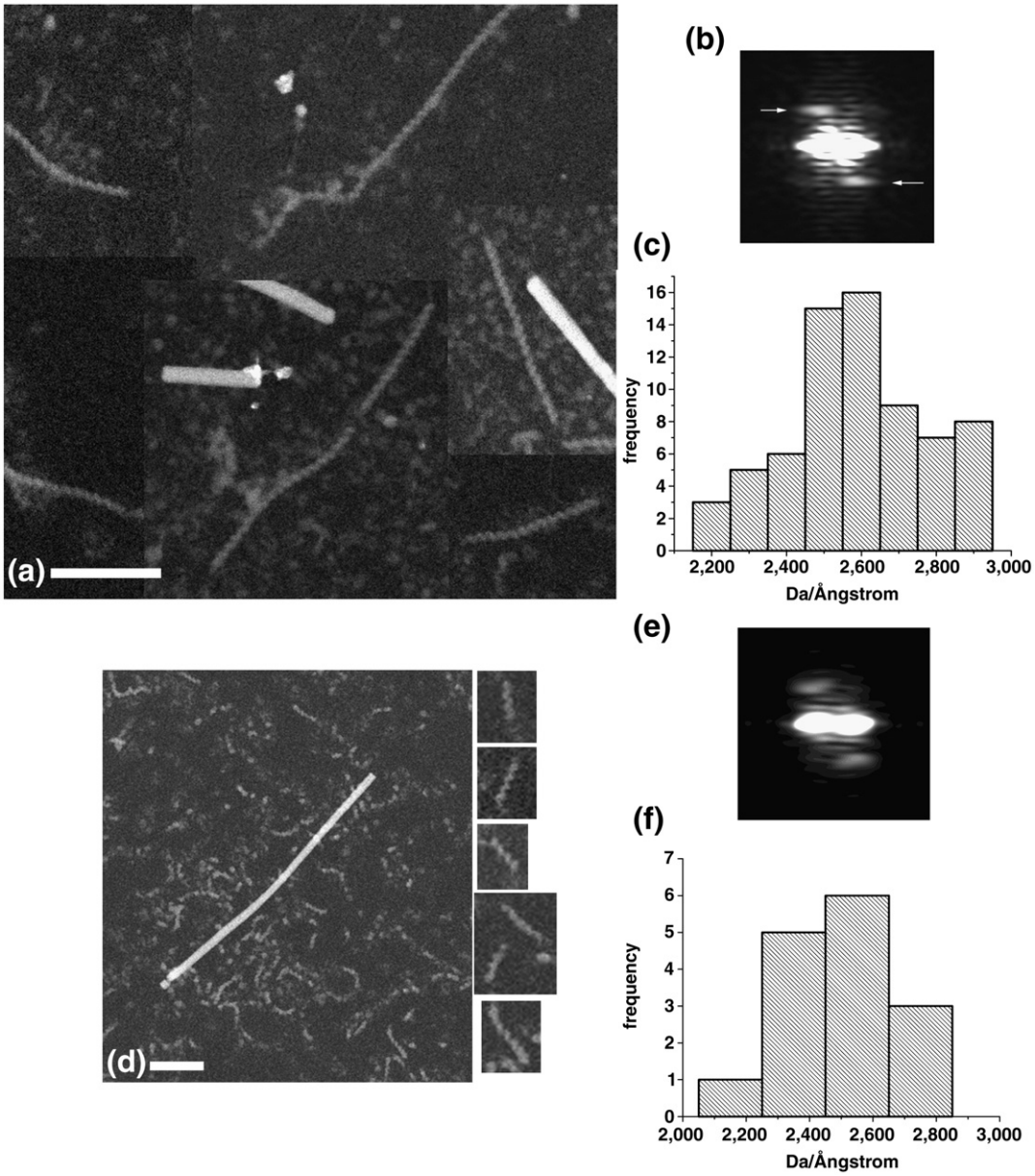


Fig. 3. A gallery (a) of unstained freeze-dried hDmc1-ssDNA-AMP-PNP filaments imaged by dark-field STEM. The more massive filaments are tobacco mosaic virus, used as a control. An averaged power spectrum (b) computed from 13 filament segments (each 500 Å long) shows a one-sided layer line (white arrows) at ~1/(100 Å). The histogram from 69 mass per unit length measurements (c) shows a mode at ~2.6 kDa/Å. A single STEM image of hDmc1-ssDNA-ATP-Ca^{2+} filaments shows that many of these filaments fall apart during preparation for imaging. However, a gallery on the right shows examples of the regions that can be used for mass analysis. An averaged power spectrum from such segments is shown (e), and the one-sided layer line is very similar to that seen in (b). The mass per unit length distribution from 15 segments displays a mode at ~2.6 kDa/Å. The scale bars (a and d) represent 1000 Å.

conventional negative staining. Glutaraldehyde fixation was tried in the STEM preparation, but the fixation led to the collapse of filaments so that no helical striations were present (data not shown). This was also consistent with previous observations.[15] Nevertheless, a limited number of segments ($n=15$) that displayed a clear helical pitch could be found. The averaged power spectrum from such segments (Fig. 3e) and the mass distribution (Fig. 3f) are shown. The average mass found was 2.5±0.2 (SD) kDa/Å, very similar to that found with AMP-PNP. While the data are sparse from STEM for this state, these STEM results are consistent with the only solutions found by image analysis (below).

Helical symmetry and three-dimensional reconstructions

The hDmc1-ssDNA-AMP-PNP filaments are more ordered than those formed with ATP and Ca^{2+}; thus, we have first used those for helical reconstruction. These filaments still have a variable pitch (Fig. 2b); hence, we used a more homogeneous subset by only using the 2554 AMP-PNP segments from the 100-Å

pitch bin in Fig. 2b for three-dimensional reconstruction. However, even when most heterogeneity is eliminated, ambiguities exist in helical reconstruction. The Iterative Helical Real Space Reconstruction method[13] is a powerful tool for such reconstructions that has been widely applied.[16] Using a starting symmetry of 6.3, 6.4, or 6.9 subunits per turn, and a featureless solid cylinder as an initial reference, the IHRSR algorithm converges (Fig. 4a) to the same structure having ~6.5 subunits per turn of a 99-Å pitch helix. We have argued previously[16] that such convergence is necessary, but certainly not sufficient, to establish that the symmetry is correct. The three-dimensional volume generated (Fig. 4c) is very similar to a crystal structure of the yeast Rad51 filament when that structure is low-pass filtered to 20 Å (Fig. 4d) and requires no rotations of the subunit as needed by Okorokov *et al.* to fit their three-dimensional reconstruction. However, when the IHRSR procedure is started from other symmetries, one can also get convergence to reconstructions that must be artifactual. It can be seen that initial symmetries of 8.3, 8.5, and 9.0 subunits per turn (Fig. 4b) all converge to a symmetry of ~8.5 subunits per turn, with the resulting reconstruction shown in Fig. 4e. Similarly, one can also get convergence to other symmetries, such as 7.4 subunits per turn (data not shown).

Can one distinguish among these results to find the correct one? We have previously shown,[16] using an example of a dynamin tube, that two different reconstructions (one with ~13 subunits per turn, the other with ~15 subunits per turn) that are indistinguishable in both their two-dimensional power spectrum and their projected image can be generated. Since the images that are recorded experimentally in the electron microscope correspond to the projection of a three-dimensional volume, there is no way that one can discriminate between these two reconstructions without additional knowledge. This additional information might come from doing tilts in the electron microscope, from STEM mass measurements, from prior knowledge of what the subunit looks like, from metal shadowing to reveal surface features, or from obtaining higher-resolution information where these ambiguities must disappear. In the case of the hDmc1-ssDNA filaments, the available resolution is simply too limited by the large disorder and variability to reveal the correct symmetry without additional information or without asking which possible solution obtained provides the best fit to existing crystal structures of Dmc1-like filaments (Fig. 4d). At a resolution of ~20 Å, the reconstruction with ~6.5 subunits per turn of a 100-Å pitch helix (Fig. 4c) provides a very good match to the Rad51 crystal filament (containing 6.0 subunits per 130 Å pitch turn). The reconstruction with ~8.5 subunits per turn (Fig. 4e), on the other hand, cannot be fit by the crystal subunit without interpenetration of neighboring subunits. Our confidence in this solution is also supported by the STEM measurements (Fig. 3c) that are consistent with ~6.5 subunits per turn. In contrast, the two reconstructions from Okorokov *et al.*[5] (Fig. 3f and g) bear no resemblance to any of the three existing crystal structures for active filaments in this family of proteins: archaeal RadA,[2] bacterial RecA,[9] and yeast Rad51.[3] More importantly, the molecular model that was used by Okorokov *et al.* to fit their reconstruction was wrong, as they assumed that the Dmc1 N-terminal domain (missing from the Dmc1 crystal structure[17]) would be on the same side of the globular core as the RecA C-terminal domain. It is actually on the opposite side of the subunit,[2,3] as shown by the N-terminal domains colored red in Fig. 4d. This should have been apparent at 20 Å resolution and quite obvious at a putative 16-Å resolution.[5]

In contrast to the AMP-PNP filaments that display convergence to different symmetries in the IHRSR procedure, the much more disordered hDmc1-ssDNA-ATP-Ca^{2+} filaments behave quite differently. Most of the variability in pitch for these ATP-Ca^{2+} filaments was eliminated by only using the 2317 segments classified in Fig. 2c as having a pitch near 100 Å (the 95- to 105-Å bin). When the IHRSR procedure was started (Fig. 5a) with a symmetry of 9.0 subunits per turn (40° rotation per subunit), convergence was achieved at ~7.4 subunits per turn (48.8°). When a starting symmetry of 8.5 subunits per turn (42.35°) was used, the procedure converged to a different final symmetry of ~7.2 subunits per turn (50.3°). The same solution was reached when one started with 8.0 subunits per turn (50.4°). However, if one used a starting symmetry close to this (7.0 subunits per turn, or 51.4°), the solution moved further away, to 6.8 subunits per turn (52.7°). It was only for a starting symmetry of 6.5 subunits per turn (55.3°) that a stable solution that did not move away from the starting twist was found. The reconstructed volume with a symmetry of 6.5 subunits per turn (Fig. 5b) looks similar to that of the AMP-PNP filament except that the mass due to the N-terminal domain (arrow, Fig. 5b) is reduced. We suggest that this is due to the flexibility of these domains in both filaments and crystals[17] and that these domains are more disordered in the ATP filaments than they are in the ones formed with AMP-PNP. It has previously been shown that for the homologous Rad51 protein, the G103E mutation leads to substantial disorder of the N-terminal domain so that most of this mass is never visualized in three-dimensional reconstructions.[8]

Discussion

We have shown that in the presence of the non-hydrolyzable ATP analog AMP-PNP, filaments formed by the hDmc1 protein on either ssDNA or dsDNA are best approximated by a symmetry of ~6.5 subunits per turn. When combined with previous measurements,[6] this means that the stoichiometry of DNA binding in both cases is either three bases or base pairs per hDmc1 subunit. In the presence of ATP and Ca^{2+}, conditions shown to

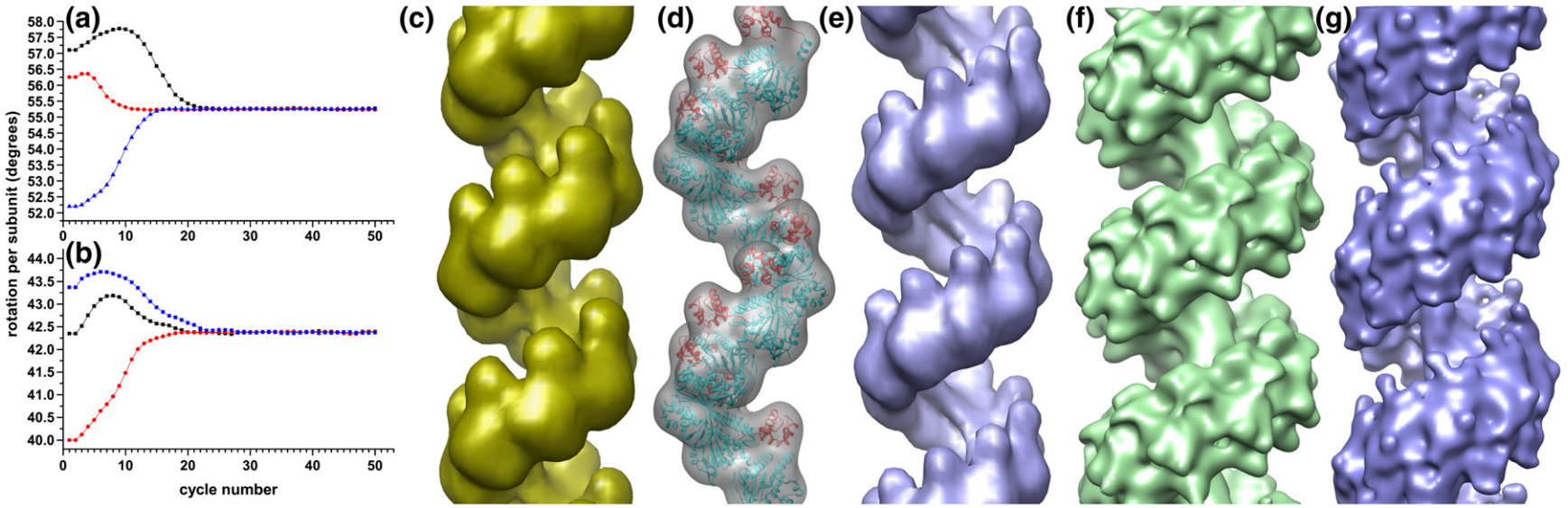


Fig. 4. The convergence of the IHRSR procedure for hDmc1-ssDNA-AMP-PNP filament segments ($n = 2554$) can be seen for starting symmetries of 6.3 (black), 6.4 (red), and 6.9 (blue) units per turn (a), as well as for 8.3 (blue), 8.5 (black) and 9.0 (red) units per turn (b). The resulting reconstruction having ~6.5 units per turn is shown in (c), while the resulting reconstruction having ~8.5 units per turn is shown in (e). For comparison, 11 subunits from a crystal structure[3] of yeast Rad51 protein are shown (d), with a surface in gray filtered to 20 Å resolution. The N-terminal domain is shown in red, while the ATP-binding core is shown in cyan. The pitch of the Rad51 crystal filament (d) is 130 Å, in contrast to the 100-Å pitch for the reconstructions (c and e). The two reconstructions from Okorokov *et al*. are also shown for comparison, one called compressed (f) and the other extended (g).

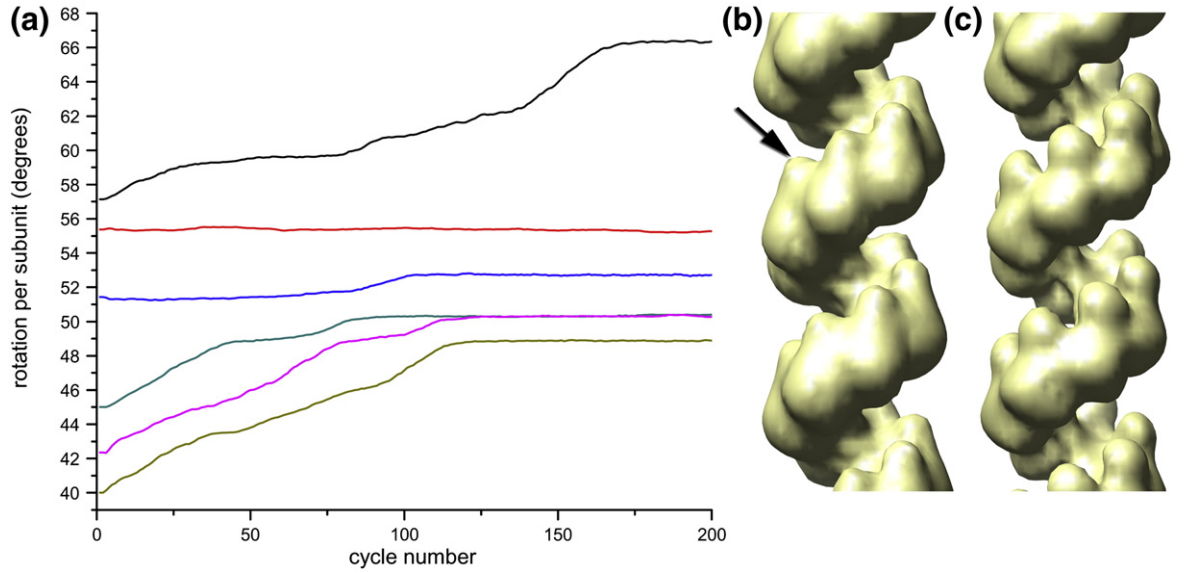


Fig. 5. The failure to see convergence (a) for a number of different starting symmetries for hDmc1-ssDNA-ATP-Ca^{2+} filaments in the IHRSR procedure shows that they behave differently from the more ordered hDmc1-ssDNA-AMP-PNP filaments (Fig. 4a). When one starts with a symmetry of 6.5 subunits per turn (55.4°, red line), the symmetry does not change over 200 iterations. The three-dimensional reconstruction with 6.5 subunits per turn after 200 iterations is shown (b), with an arrow indicating the feature due to the N-terminal domain. It can be seen in the comparison with the hDmc1-ssDNA-AMP-PNP reconstruction (c) that the mass due to the N-terminal domain is substantially reduced in the more disordered filaments formed with ATP and Ca^{2+}.

produce active hDmc1-DNA filaments,[15] filaments on ssDNA are substantially more disordered than those formed with AMP-PNP. Nevertheless, analysis of these disordered filaments suggests that they have the same helical symmetry (~6.5 subunits per helical turn) and therefore the same DNA-binding stoichiometry (3 bases per subunit) as those formed with AMP-PNP. While we cannot exclude that the filaments examined by Okorokov *et al.* might actually have ~9 subunits per turn, a much more likely explanation, given all that we now know, is that their result arose from a potential ambiguity present in helical reconstruction.

The cautionary message of this paper is to raise a greater awareness that helical reconstructions, generated using either Fourier–Bessel methods[18] or real-space approaches,[19] can suffer from multiple solutions at limited resolution that are all equally consistent with the images used to generate these reconstructions. Since only one of these solutions can be correct, disambiguation is required, which might use prior knowledge about the structure of the subunit, mass per length measurements, or tilts of filaments in the microscope. In the absence of such additional information, a burden should exist to show that the proposed solution is indeed unique.

Materials and Methods

Sample preparation

The hDMC1-ssDNA-AMP-PNP complexes were formed in 25 mM triethanolamine–HCl (Fisher) buffer (pH 7.2) with a 20-min incubation at 37 °C. The hDMC1 (2 μM) was in a ratio of 80:1 (w/w) to a synthesized 108-base single-stranded oligonucleotide. AMP-PNP (Sigma) (2.5 mM), magnesium acetate (Sigma) (2 mM), and potassium chloride (J. T. Baker) (200 mM) were present. The hDMC1-dsDNA-AMP-PNP complexes were formed under the same conditions, except that calf thymus dsDNA (Sigma) was used instead at a 1:40 ratio (w/w) to the hDmc1.

The hDMC1-ssDNA-ATP-Ca^{2+} complexes were formed in 25 mM triethanolamine–HCl (Fisher) buffer (pH 7.2) with a 20-min incubation at 37 °C. The hDMC1 (2 μM) was in a ratio of 80:1 (w/w) to a synthesized 108-base single-stranded oligonucleotide. ATP (Sigma) (2.5 mM), calcium chloride (J. T. Baker) (2 mM), sodium chloride (Fisher) (50 mM), and DTT (Sigma) (1 mM) were present. When fixation was used for STEM, a fresh electron-microscopy-grade aqueous glutaraldehyde (Electron Microscopy Sciences) was then added into the solution to a final concentration of 0.2% and incubated at 37 °C for 15 min.

Samples were applied to glow-discharged carbon-coated grids and stained with 2% uranyl acetate (w/v) for transmission electron microscopy. Images were recorded on film with a Tecnai 12 electron microscope operating at 80 keV with a nominal magnification of 30,000×. Negatives were scanned with a Nikon Coolscan 8000 densitometer at a raster of 4.16 Å/pixel.

Samples for STEM were prepared as previously described.[20] Digital dark-field micrographs of the freeze-dried samples were recorded in 512×512 frames at either 1.0 or 2.0 nm/pixel at the Brookhaven STEM Facility. Images were analyzed using PCMass 3.0.

Image analysis and reconstruction

Filaments were boxed using the *helixboxer* program within EMAN.[21] These filaments were then cut into

overlapping boxes that were 74 pixels long, and padded to 74 pixels width. The SPIDER software package[22] was used for most operations. Global three-dimensional reconstructions of each form (dsDNA-AMP-PNP, ssDNA-AMP-PNP, and ssDNA-ATP-Ca^{2+}) were generated using the IHRSR procedure[13] but forcing the axial rise to be fixed at 1.0 Å. This led to a stable solution with the rotation per subunit of ~3.6°, so that there was one helical turn every ~100 subunits or 100 Å. These reconstructed volumes were then continuously deformed to have different pitches, and these new volumes were then used as references for sorting. The "reference-free" averages were created using the AP SR procedure within SPIDER. Averaged power spectra were generated by padding each segment to 512×512 pixels, taking the fast Fourier transform of the padded image, and then adding the modulus squared of each Fourier transform together. This procedure is thus invariant under any translations of the segments.

Acknowledgements

We thank Beth Lin and Joe Wall of the Brookhaven STEM Facility for preparing grids and imaging them. We thank Doug Bishop for the generous gift of human Dmc1 protein. This work was supported by National Institutes of Health grants GM035269 and EB001567.

References

1. Roca, A. I. & Cox, M. M. (1997). RecA protein: structure, function, and role in recombinational DNA repair. *Prog. Nucleic Acid Res. Mol. Biol.* **56**, 129–223.
2. Wu, Y., He, Y., Moya, I. A., Qian, X. & Luo, Y. (2004). Crystal structure of archaeal recombinase RADA: a snapshot of its extended conformation. *Mol. Cell*, **15**, 423–435.
3. Conway, A. B., Lynch, T. W., Zhang, Y., Fortin, G. S., Fung, C. W., Symington, L. S. & Rice, P. A. (2004). Crystal structure of a Rad51 filament. *Nat. Struct. Mol. Biol.* **11**, 791–796.
4. Bishop, D. K., Park, D., Xu, L. & Kleckner, N. (1992). DMC1: a meiosis-specific yeast homolog of *E. coli* recA required for recombination, synaptonemal complex formation, and cell cycle progression. *Cell*, **69**, 439–456.
5. Okorokov, A. L., Chaban, Y. L., Bugreev, D. V., Hodgkinson, J., Mazin, A. V. & Orlova, E. V. (2010). Structure of the hDmc1-ssDNA filament reveals the principles of its architecture. *PLoS ONE*, **5**, e8586.
6. Sheridan, S. D., Yu, X., Roth, R., Heuser, J. E., Sehorn, M. G., Sung, P. *et al.* (2008). A comparative analysis of Dmc1 and Rad51 nucleoprotein filaments. *Nucleic Acids Res.* **36**, 4057–4066.
7. VanLoock, M. S., Yu, X., Yang, S., Lai, A. L., Low, C., Campbell, M. J. & Egelman, E. H. (2003). ATP-mediated conformational changes in the RecA filament. *Structure (London)*, **11**, 187–196.
8. Galkin, V. E., Wu, Y., Zhang, X. P., Qian, X., He, Y., Yu, X. *et al.* (2006). The Rad51/RadA N-terminal domain activates nucleoprotein filament ATPase activity. *Structure*, **14**, 983–992.
9. Chen, Z., Yang, H. & Pavletich, N. P. (2008). Mechanism of homologous recombination from the RecA-ssDNA/dsDNA structures. *Nature*, **453**, 489–494.
10. Li, Z., Golub, E. I., Gupta, R. & Radding, C. M. (1997). Recombination activities of HsDmc1 protein, the meiotic human homolog of RecA protein. *Proc. Natl Acad. Sci. USA*, **94**, 11221–11226.
11. Passy, S. I., Golub, E. I., Golub, E. I., Golub, E. I., Golub, E. I., Golub, E. I. & Golub, E. I. (1999). Human Dmc1 protein binds DNA as an octameric ring. *Proc. Natl Acad. Sci. USA*, **96**, 10684–10688.
12. Penczek, P. A., Radermacher, M. & Frank, J. (1992). Three-dimensional reconstruction of single particles embedded in ice. *Ultramicroscopy*, **40**, 33–53.
13. Egelman, E. H. (2000). A robust algorithm for the reconstruction of helical filaments using single-particle methods. *Ultramicroscopy*, **85**, 225–234.
14. Wall, J. S. & Hainfeld, J. F. (1986). Mass mapping with the scanning transmission electron microscope. *Annu. Rev. Biophys. Biophys. Chem.* **15**, 355–376.
15. Bugreev, D. V., Golub, E. I., Stasiak, A. Z., Stasiak, A. & Mazin, A. V. (2005). Activation of human meiosis-specific recombinase Dmc1 by Ca^{2+}. *J. Biol. Chem.* **280**, 26886–26895.
16. Egelman, E. H. (2007). The iterative helical real space reconstruction method: surmounting the problems posed by real polymers. *J. Struct. Biol.* **157**, 83–94.
17. Kinebuchi, T., Kagawa, W., Enomoto, R., Tanaka, K., Miyagawa, K., Shibata, T. *et al.* (2004). Structural basis for octameric ring formation and DNA interaction of the human homologous-pairing protein Dmc1. *Mol. Cell*, **14**, 363–374.
18. DeRosier, D. J. & Klug, A. (1968). Reconstruction of three-dimensional structures from electron micrographs. *Nature*, **217**, 130–134.
19. Egelman, E. H. (2007). Single-particle reconstruction from EM images of helical filaments. *Curr. Opin. Struct. Biol.* **17**, 556–561.
20. Wall, J. S., Simon, M. N., Lin, B. Y. & Vinogradov, S. N. (2008). Mass mapping of large globin complexes by scanning transmission electron microscopy. *Methods Enzymol.* **436**, 487–501.
21. Ludtke, S. J., Baldwin, P. R. & Chiu, W. (1999). EMAN: semiautomated software for high-resolution single-particle reconstructions. *J. Struct. Biol.* **128**, 82–97.
22. Frank, J., Radermacher, M., Penczek, P., Zhu, J., Li, Y., Ladjadj, M. R. & Leith, A. (1996). SPIDER and WEB: processing and visualization of images in 3D electron microscopy and related fields. *J. Struct. Biol.* **116**, 190–199.